An Experimental Evaluation of Popular Image Parameters for Monochromatic Solar Image Categorization

Juan M. Banda, Rafal A. Angryk

Department of Computer Science
Montana State University,
Bozeman, MT, 59715 USA.
{juan.banda, angryk}@cs.montana.edu

Abstract

In this work, we perform experimental evaluation of different image parameters, from the perspective of large-scale content-based discovery of solar phenomena in NASA images. Many of the recently published papers, often from different areas of application (e.g. medical, military images), describe different parameters for image recognition and state high quality of the generated results. Overwhelmed with the number of proposed image parameters, and concerned with their practical applicability to large-scale solar data analysis, we decided to perform our own comparative analysis of these parameters. Because of the lack of broadly accepted Solar Images benchmark data sets, in this paper we introduce our own benchmark created using solar images registered during the TRACE mission. Using the first solar domain-specific benchmark data set that contains multiple types of phenomena, we investigate the correlation of different image parameters and their importance from the perspective of distinguishing between different types of solar phenomena. In this paper, we present recommendations on the image parameters that perform adequately for the solar data.

1 Introduction

In this work, we present the first step toward the ambitious goal of building a Content Based Image Retrieval (CBIR) system for the Solar Dynamics Observatory (SDO) mission [25]. Our motivation behind this work is that based on the amounts of data that the SDO mission will be transmitting. Hand labeling of these images would be an impossible task.

The SDO with its Atmospheric Imaging Assembly (AIA) is expected to generate at least one set of eight 4096 pixels x 4096 pixels images every 10 seconds. This will lead to a data transmission rate of $2.1*10^8$ bits per second (i.e. approx. 700 Gigabytes/day) only from the AIA component (the entire mission is expected to be sending about 1.5 Terabytes of data per day, for a minimum of 5 years) [25]. There have been several successful CBIR systems for medical images [9] as well as in other domains [7]; none of them, however, have dealt with the volume of data that the SDO mission will generate.

We decided to take a systematic approach to our work and start with the creation of a benchmark data set that includes multiple types of solar phenomena images, all in a balanced distribution. Many of the benchmarks published in the solar physics community reflect interests of individual physicists, who tend to specialize in one type of phenomena. To our best knowledge, our benchmark data set is the first one that spans eight types of phenomena. Since the SDO mission has not launched yet, we used images from the TRACE repository to create our data set. These images feature a similar format to the ones the SDO mission will generate.

By segmenting our images we can better identify areas that present solar activity. Instead of analyzing the whole image, this will also make the recognition process more rotation-resistant. SDO images will have a resolution of 4096 x 4096 pixels and will be "Full Disk" (a.k.a "Full Sun"), so we could not risk extracting the image parameters of the whole image without taking into consideration that the solar phenomena only occurs in part of the image and the rest of the image data will be very similar to images with no solar activity, labeled in our data set as "Empty Sun".

We extract image parameters for individual grid cells believing that individual types of solar activity will present different values for them. The majority of our feature parameters are texture-based and selected based on previous work [1, 16] that showed promising results when they were applied to solar images. We are also testing other parameters that have been used in previous research [9], for images in other domains. One of the main goals of this work is to determine which image parameters we can safely remove while maintaining high quality parameter-based representation of original solar images.

We decided to start our work on the CBIR system by investigating the correlation of extracted image parameters. Our decision behind using a correlation comparison is based on the premise that we can achieve dimensionality reduction by finding strongly correlated (i.e redundant) image parameters. The use of statistical analysis seems to be more accepted within the astrophysics community than heuristics and supervised dimensionality reduction techniques. The correlation based approach was also a starting point in the development of CBIR systems for other domains [9].

Our goal of publishing this work is to obtain valuable feedback from the community, especially from astrophysicists using image parameters other than the ones presented. We are looking forward to building new

collaborations with domain experts that are working on identifying individual solar phenomena, and see what else we can add to our benchmark data set and the CBIR system in order to better serve its purpose.

2 Background

2.1 Activity in the solar community

Automatically detecting individual phenomena in solar images has become a popular topic in recent years. Zharkova et al. [32] discuss several methods for identifying phenomena in solar images including artificial neural networks, bayesian interference, and shape correlation and analize five different phenomena: sunspots, inference, plage, coronal mass ejections, and flares. Automatic identification of flares, on the SDO mission, will be performed by an algorithm created by Christe et al. [6] which works well for noisy and background-affected light curves. Filament detection for the SDO mission will be implemented using the "Advanced Automated Filament Detection and Characterization Code" [2]. This algorithm goes beyond the typical filament identification; it determines its spine and orientation angle, finds its magnetic chirality (sense of twist), and tracks it from image to image for as long as they are visible on the solar disk. As for the coronal jet detection and parameter determination algorithms, they will work on data cubes covering a box enclosing the bright point and extending forward in time. SDO methods for determining the coronal jet parameters are described in detail in [23]. Oscillations on the SDO pipeline will be detected using algorithms presented in [8] and [19] that consist of wavelet transform analysis. In order to detect active regions, the SDO pipeline will use the Spatial Possibilistic Clustering Algorithm (SPoCA). This algorithm produces a segmentation of EUV solar images into classes corresponding to active region, coronal hole and quiet sun.

As we can clearly see, the majority of currently popular approaches deal with the recognition of individual phenomena and a few of them have demanding computational costs. Not until recently, Lamb et al. [16] discussed creating an example based Image Retrieval System for the TRACE repository. This is the only attempt we are aware of that involves trying to find a variety of phenomena, with expectation of building a large-scale CBIR system for solar physicists.

2.2 Image parameters

Based on our literature review, we decided that we would analyze some of the most popular image parameters used in different fields such as medical images [4, 9, 13, 14], text recognition [31], natural scene images [5, 10, 15, 22], traffic images [30], and texture images [18, 20, 27]. As a common denominator, the usefulness of all these image parameters have shown to be very domain dependent.

The ten image parameters that we extracted are: the Mean intensity, the Standard Deviation of the intensity, the Third Moment and Fourth Moment, Uniformity, Entropy, and Relative Smoothness, Fractal Dimension [24], and two Tamura texture attributes: Contrast and Directionality [26]. All of the attributes above can be extracted from the images quickly - an important aspect when dealing with large sets of solar images.

Our decision on dropping computationally expensive image parameters comes our previous work [1] and the fact that we will have to process data in almost real time when the SDO mission is launched (i.e. the rate of eight 4096x4096 images per every 10 seconds), so we will have a very small amount of time to be able to extract all the image parameters.

3 Approach

3.1 Benchmark data set creation

Our data set was created using the Heliophysics Events Knowledgebase (HEK) portal [12] to find the event dates. Then we retrieved the actual images using the TRACE Data Analysis Center's catalog search [28]. The search extends into the TRACE repository as well as other repositories. To make all images consistent, we filtered out all results that did not came from the TRACE mission. Table 1 provides an overview of our data set. All images selected have an extent label of "Partial Sun" (were taken from a section of the sun).

In the process of creating our data set to analyze parameters for image recognition, we stumbled upon several problems when trying to balance the number of images per class. First, we found that several phenomena do not occur as often as others, making it harder to balance the number of images between individual classes. The second issue is that several phenomena can be sighted and reported in different wavelengths, for our benchmark we selected the wavelengths that contained the largest number of hand labeled results provided by HEK [12] contributors. Finally, noticed that some of the retrieved had different (768x768) resolution than the most common 1024x1024. Since the resizing did not modify their histograms, we decided to increase the resolution of those few images, so our entire benchmark data set could be processed in the same manner.

All events retrieved were queried within the 99-11-03 to 08-11-04 date ranges. As you can see from the table 1, for the 16 events searchable by HEK, we had to reduce the number of events to 8, due to the limited number of available occurrences of the remaining types of phenomena, and poor quality of images available in some of the data catalogs. The current selection of classes was solely based on the number of images available, and the wavelengths in which the images where available. We wanted to be sure that our benchmark data set has equally frequent classes in order to be sure that our results are not skewed towards the most frequent phenomena. For the events that occurred only a few times, but during a prolonged period of time, we have selected a few different images within that time range to complete our goal of 200 images per event class.

Table 1: Characteristics of our benchmark data set [33]

Event Name	# of images retrieved	Wave-length	Resolution (count)	HEK reported events
Active Region	200	1600	768x768 (200)	200+
Coronal Jet	200	171	1024x1024 (155) 768x768 (45)	25
Emerging Flux	200	1600	768x768 (200)	12
Filament	200	171	1024x1024 (127) 768x768 (73)	45
Filament Activation	200	171	1024x1024 (200)	27
Filament Eruption	200	171	1024x1024 (49) 768x768 (151)	53
Flare	200	171	1024x1024 (64) 768x768 (136)	200+
Oscillation	200	171	1024x1024 (50) 768x768 (150)	3

In the end of this step, we have a benchmark data set of 1,600 images with 200 images per event class. The benchmark data set in its original format is available to the public via Montana State University's Server [33]. Because of promising results obtained during our preliminary investigation [1] and the work of other members of our team [16], we chose to segment our images using an 8 by 8 grid for our image parameter extraction and labeling, resulting in 102,400 cells. For the labeling of our images, we used the HER VOEvent XML data that indicate the regions within the images where the events occur. We only labeled the grid cells that overlap with that region with the event name. All other grid cells not included within the region where labeled as "Empty Sun". Despite different frequencies of labeled cells, we used even sampling methods when conducting our experiments.

3.2 Image parameter extraction:

Once our data set was completely formed during our first experiments, we noticed that few of the parameters we obtained from the literature needed to be discarded due to their extensive computational costs.

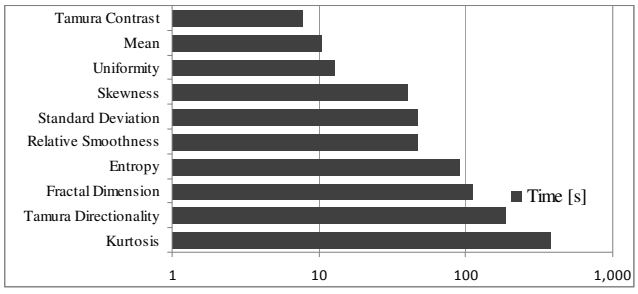

Figure 1: Time needed to generate popular texture parameters for 102,400 cells in the entire benchmark data set [33].

Please note that these image parameters are not exhaustive and there are a very large number of other parameters that we could have tested. We have selected our image parameters based on previous work in solar images [17] and other works listed in section 2.2. Since almost every day new image parameters are being published by professionals working in the field of image processing, testing everything would be a daunting task. One of our future goals is to add more parameters, and we are looking forward to obtaining recommendations from the solar community.

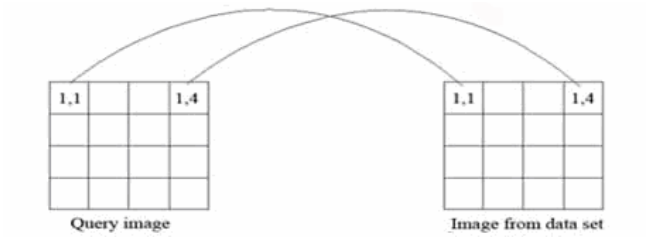

Figure 2: One-to-one comparison between the query image (q_l) cells against images from the benchmark cells (X_n). Cell 1,1 will only be compared to the cell 1,1 and so on.

3.3 Correlation-based evaluation of image parameters

Automatic methods for image parameter selection have been proposed in [21, 29]. However, these automatic methods do not directly explain why features are chosen. The method proposed in [9] analyzes correlations between the values of the parameters themselves, and instead of automatically selecting a set of features, provides the user with information to help them select an appropriate set of features. In order to determine the usefulness of our features, we decided to utilize this approach, allowing us to determine which features are redundant.

To analyze the correlation between different image parameters, we evaluate the correlation between the Euclidean distances $d(q,X)$ obtained for each image parameter of each of the images X from our benchmark given any query image q. For each pair of query image q and benchmark image X, we create a vector $(d_1(q,X), d_2(q,X),...d_m(q,X),....d_M(q,X))$ where $d_m(q,X)$ is the distance of the query image q to the benchmark image X for the $_m$th image parameter, and M is the total number of image parameters. Then we calculate the correlation between d_m over all queries $q = \{q_1,..., q_l,...q_L\}$ and all images $X = \{X_1,...,X_m,...,X_N\}$. The $M \times M$ covariance matrix, denoted as Σ_{ij}, of the d_m is calculated over all N database images and all L query images as:

$$\Sigma_{ij} = \frac{1}{NL}\sum_{n=1}^{N}\sum_{l=1}^{L}(d_i(q_l, X_n) - \mu_i)\cdot d_j(q_l, X_n) - \mu_j) \quad (1)$$

$$\text{with } \mu_i = \frac{1}{NL}\sum_{n=1}^{N}\sum_{l=1}^{L} d_i(q_l, X_n) \quad (2)$$

By segmenting each of our images into 64 grid cells, the number of queries we have is equal to the number of grid cells. The grid cells are compared based on an exact one to one match (query(r,c) vs image$N(r,c)$ where r is row and c is column) within the images for each image parameter. Comparing one to all is very computationally expensive, since we would have to compare 64 cells in the query (per

image parameter), against the 64 cells in the images from our benchmark doing 64x64 comparisons per image parameter times the number of parameters. Figure 2 shows how the one-to-one grid cell comparison was performed.

Given the covariance matrix $\sum_{ij}$, we calculate the correlation matrix R_{ij}. A high value r_{ij} means a high similarity between features i and j. This correlation matrix can then be analyzed to find out which of our parameters have highly correlated values and which do not.

4 Experimental Results

Based on the image parameter evaluation method outlined on section 3.3, in one scenario we randomly selected a query image from each class and analyzed the correlation between this image and the rest of the images of the same class in order to observe which image parameters are strongly correlated and which ones are not within the same class. In the second scenario, we analyzed the correlation between the query images and the rest of the images of the same wavelength from all other classes in order to observe which image parameters feature similar correlation to the rest of the classes than to the same class.

We believe that the intra-class correlation (the first scenario above) should be of interest for astrophysics specializing in individual types of phenomena (allowing them to not be concerned with the extraction of image parameters that are highly correlated), whereas inter-class correlation (the second scenario) interested us the most.

Since Active Regions are some of the most distinguishable classes to discover in our benchmark data set and they are also one of the basic indicators of solar activity occurrence, we decided to start our investigation by analyzing the correlations between query images of this class.

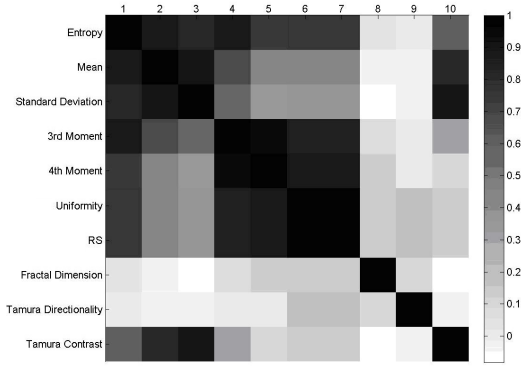

Figure 3: Average correlation map for the Active Region class in the one image as a query against the same class scenario (intra-class correlation).

From figure 3, we can clearly see two image parameters that are weakly correlated against pretty much every other parameter: Fractal Dimension and Tamura Directionality. In the strongly correlated section we have: Entropy, 3rd moment and 4th moment with Uniformity and RS, Uniformity with RS and Tamura Contrast with Standard Deviation and Mean. Due to the paper size limitations, we only present one correlation map for one of the 8 classes that we analyzed. More experimental results and an extended version of this work can be found at [33].

Since the correlation differences are not that visible from the correlation maps, we decided to use Multi Dimensional Scaling (MDS) [3] to better visualize our correlations. Close parameters in MDS maps indicate strong correlation and the more distant they are the weaker their correlation. For all the MDS maps we replaced the class name with its corresponding number (as seen in figure 3).

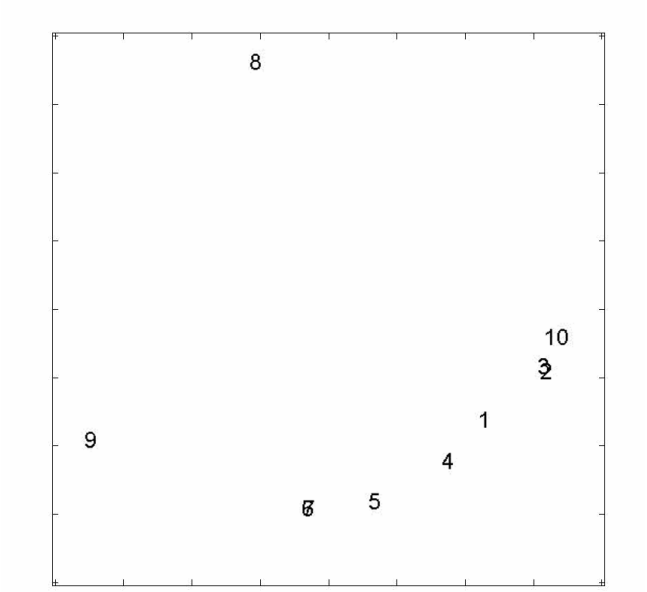

Figure 4: Multi Dimensional Scaling of correlation map from Fig. 3.

As we can see from the multi dimensional scaling maps in figure 4, it is easier to identify clusters of highly correlated image parameters (their numbers are overlapping), and the less correlated parameters can be found on the edges of the map.

Based on the correlation maps and the multi dimensional scaling maps, we were able to perform a wide variety of experiments using classifiers in order to determine if we could attempt any dimensionality reduction to save our storage space and computing costs. Table 2 presents three different experimental scenarios that we performed for continuing our investigation on the Active Region class.

Table 2: Name of the experiment and the settings used

Name	Experiment Settings
Exp 1	Original ten image parameters
Exp 2	Removing 3 uncorrelated parameters: Fractal Dimension, Tamura Directionality and Contrast (numbers 8,9,10 in figures 3 and 4)
Exp 3	Removing 3 parameters that are highly correlated to others: Standard Deviation, Uniformity and Tamura Contrast (numbers 3,6,10 in figures 3 and 4)

We selected two linear classifiers, Support Vector Machines (SVM) and Naïve Bayes, as well as one decision tree based classifier, C4.5. We also used Adaboost on our best performing classifier in order to improve our results (denoted as ADA C45 in Tab. 3). For our experiments with the classifiers, we used the standard 10 fold cross validation, with an even distribution of labeled cells. In order to achieve this we took the minimum amount of labeled cells for all classes, in data set Emerging Flux has 1,552 instances, and selecting randomly that amount of labeled cells from images of the other classes. This gave us a total of 13,968 instances to work on (exactly 1,552 per each of the 9 labels).

Table 3: Percentages of correctly classified instances by our selected classifiers

	Naïve Bayes	SVM	C45	ADA C45
Exp 1	31.65%	40.45%	65.60%	72.41%
Exp 2	28.59%	34.84%	59.26%	63.86%
Exp 3	33.23%	39.50%	63.55%	69.49%

As you can see from table 3, the switch from linear function based classifiers (Naïve Bayes and SVM) to decision tree based classifiers provided a considerable improvement. Here we find that the behavior of our data from the image parameters is better modeled using a decision tree like structure rather than a linear combination of the features.

Exp 2, in table 3, shows the accuracy decreases when we remove uncorrelated image parameters, and that these parameters are probably some of the most useful ones for our Image Retrieval task. Since by removing the parameters: Fractal Dimension, Tamura Directionality and Contrast we decrease our classification percentage, we can conclude that we should leave them for future experiments.

Exp 3, on table 3, shows that if we remove the 3 parameters that are strongly correlated to some of the other parameters that were kept in our data space we can almost maintain our original accuracy.

5 Conclusions

Because of the correlation analysis and the classification results, we can conclude that we can safely (i.e. without significant decrease in the quality of our image recognition system) remove up to 30% of our proposed image parameters and still achieve very similar classification results. This will let us reduce data dimensionality and storage space and computational costs for our system.

By analyzing both correlation maps and MDS maps for the rest of the classes (not presented here, but available on-line [33]), we can determine which image parameters can be removed for each class. We believe that these results are very useful for solar researchers, who usually specialize in one type of phenomena. Publication of these maps will allow any specialists to determine which image parameters are more useful for them if they are trying to focus on recognition of a certain class.

6 Future work

In this work we presented results for one class of phenomena. However, exhaustive experimentation for this and the remaining classes contained in our data set has been performed, and the Correlation and MDS maps can be found on [33]. We are still working on adding more image parameters to our vector, and we plan to analyze them in the same manner as presented here in order to determine their importance to our task.

Like we mentioned before, by adding more image parameters to evaluate, we will be able to expand the work presented in this paper and will be able to provide better recommendations in selecting the best combination of image parameters for classification purposes.

Finally, we are working on adding more classes to our benchmark and increasing the number of images in different wavelengths. If there are any other repositories of benchmarks for a particular class not listed in this work we would gladly appreciate information about them from the readers, so we could incorporate them to our benchmark data set and run our experiments with the new data. This is an on-going process that we expect will help us achieve our goal of constructing a successful CBIR system for the SDO mission. We plan to publish updates on our work in [33].

7 Acknowledgments

This work was supported in part by the NASA Grant Award No. 08-SDOSC08-0008, funded from NNH08ZDA001N-SDOSC: Solar Dynamics Observatory Science Center solicitation.

8 References

[1] J.M Banda and R. Angryk "On the effectiveness of fuzzy clustering as a data discretization technique for large-scale classification of solar images" *Proceedings of the 18th IEEE International Conference on Fuzzy Systems (FUZZ-IEEE '09),* Jeju Island, Korea, August 2009, pp. 2019-2024.

[2] P. N. Bernasconi, D. M. Rust, and D. Hakim. "Advanced Automated Solar Filament Detection And Characterization Code: Description, Performance, And Results". *Sol. Phys.*, May 2005, pp. 228:97–117.

[3] I. Borg, and P. Groenen, *Modern Multidimensional Scaling: theory and applications* (2nd ed.), Springer-Verlag New York, 2005

[4] E. Cernadas, P. Carriön, P. Rodriguez, E. Muriel, and T. Antequera. "Analyzing magnetic resonance images of Iberian pork loin to predict its sensorial characteristics" *Comput. Vis. Image Underst* 98, 2, May 2005, pp. 345-361. DOI= http://dx.doi.org/10.1016/j.cviu.2004.08.004

[5] B. B. Chaudhuri, Nirupam Sarkar, "Texture Segmentation Using Fractal Dimension," *IEEE Transactions on Pattern Analysis and Machine Intelligence,* vol. 17, no. 1, Jan. 1995, pp. 72-77. doi:10.1109/34.368149

[6] S. Christe, I. G. Hannah, S. Krucker, J. McTiernan, and R. P. Lin. “RHESSI Microflare Statistics. I. Flare-Finding and Frequency Distributions”. *ApJ* 677, April 2008, pp. 1385–1394

[7] R. Datta, J Li and Z Wang. Content-based Image Retrieval – Approaches and Trends of the New Age. In: *ACM Intl. Workshop on Multimedia Information Retrieval, ACM Multimedia.* Singapore; 2005.

[8] I. De Moortel and R. T. J. McAteer. “Waves and wavelets: An automated detection technique for solar oscillations”. *Sol. Phys*. 223, September 2004, pp. 1–2.

[9] T. Deselaers, D. Keysers, and H. Ney, "Features for Image Retrieval: An Experimental Comparison", *Information Retrieval, vol. 11, issue 2*, The Netherlands, Springer, March 2008, pp. 77-107.

[10] V. Devendran, T. Hemalatha, W. Amitabh "SVM Based Hybrid Moment Features for Natural Scene Categorization," *International Conference on Computational Science and Engineering* vol. 1, 2009, pp.356-361.

[11] R.C. Gonzalez, and R. E. Woods, *Digital Image Processing*. (2nd ed.), Addison-Wesley Longman Publishing Co., Inc. 2001

[12] Heliophysics Event Registry [Online] Available: http://www.lmsal.com/~cheung/hpkb/index.html [Accessed: Jan 24, 2010]

[13] S.S. Holalu and K. Arumugam “Breast Tissue Classification Using Statistical Feature Extraction Of Mammograms”, *Medical Imaging and Information Sciences*, Vol. 23 No. 3, 2006, pp. 105-107.

[14] H.F. Jelinek, D.J. Cornforth, A.J. Roberts, G. Landini, P. Bourke, and A. Iorio, “Image processing of finite size rat retinal ganglion cells using multifractal and local connected fractal analysis”, *In 17th Australian Joint Conference on Artificial Intelligence, volume 3339 of Lecture Notes in Computer Science,* Springer--Verlag Heidelberg, 2004, pp 961-966.

[15] S. Kulkarni, B. Verma, "Fuzzy Logic Based Texture Queries for CBIR," *Fifth International Conference on Computational Intelligence and Multimedia Applications (ICCIMA'03)*, 2003, pp.223

[16] R. Lamb, “An Information Retrieval System For Images From The Trace Satellite,” *M.S. thesis,* Dept. Comp. Sci., Montana State Univ., Bozeman, MT, 2008.

[17] R. Lamb, R. Angryk, and P. Martens, "An Example-based Image Retrieval System for the TRACE Repository", *Proceedings of the 19th International Conference on Pattern Recognition (ICPR '08)*, Tampa, FL, USA.

[18] H Lin, C Chiu, and S. Yang, “LinStar texture: a fuzzy logic CBIR system for textures”, *In Proceedings of the Ninth ACM international Conference on Multimedia* (Ottawa, Canada, September 30 - October 05, 2001). MULTIMEDIA '01, vol. 9. ACM, New York, NY, pp. 499-501. DOI= http://doi.acm.org/10.1145/500141.500223

[19] R. T. J. McAteer, P. T. Gallagher, D. S. Bloomfield, D. R. Williams, M. Mathioudakis, and F. P. Keenan. “Ultraviolet Oscillations in the Chromosphere of the Quiet Sun”. *ApJ*, 602, February 2004, pp. 436–445.

[20] J. Muwei, L. Lei, G. Feng, "Texture Image Classification Using Perceptual Texture Features and Gabor Wavelet Features," *Asia-Pacific Conference on Information Processing* vol. 2, 2009, pp.55-58

[21] M. Najjar, C. Ambroise, J.P Cocquerez, “Feature Selection For Semi Supervised Learning Applied To Image Retrieval” In*: ICIP 2003*. vol. 3. Barcelona, Spain; 2003. p. 559–562.

[22] A.P Pentland, “Fractal-based description of natural scenes’, *IEEE Trans. on Pattern Analysis and Machine Intelligence* 6, 1984, pp. 661-674.

[23] A. Savcheva, J. Cirtain, E. E. Deluca, L. L. Lundquist, L. Golub, M. Weber, M. Shimojo, K. Shibasaki, T. Sakao, N. Narukage, S. Tsuneta, and R. Kano. “A Study of Polar Jet Parameters Based on Hinode XRT Observations”. *Publ. Astron. Soc*. Japan, 59, November 2007, pp. 771–+.

[24] M. Schroeder. *Fractals, Chaos, Power Laws: Minutes from an Infinite Paradise.* New York: W. H. Freeman, 1991, pp. 41-45.

[25] Solar Dynamics Observatory [Online], Available: http://sdo.gsfc.nasa.gov/. [Accessed: Sep 29, 2009]

[26] H. Tamura, S. Mori, T. Yamawaki. “Textural Features Corresponding to Visual Perception”. *IEEE Transaction on Systems, Man, and Cybernetics* 1978;8(6): pp. 460–472.

[27] S. Thumfart, W. Heidl, J. Scharinger, and C/ Eitzinger. “A Quantitative Evaluation of Texture Feature Robustness and Interpolation Behaviour”. In *Proceedings of the 13th international Conference on Computer Analysis of Images and Patterns* (Münster, Germany, September 02 - 04, 2009).

[28] TRACE On-line (TRACE) [Online], Available: http://trace.lmsal.com/. [Accessed: Sep 29, 2009]

[29] N. Vasconcelos, M. Vasconcelos, ”Scalable Discriminant Feature Selection for Image Retrieval and Recognition” In *CVPR 2004*. 2. Washington, DC, USA; 2004. p. 770–775.

[30] C. Wen-lun, S. Zhong-ke, F. Jian, "Traffic Image Classification Method Based on Fractal Dimension," *IEEE International Conference on Cognitive Informatics* Vol. 2, 2006 5th, pp.903-907.

[31] S. T. Wong, H. Leung, and H. H. Ip, “Model-based analysis of Chinese calligraphy images” *Comput. Vis. Image Underst.* 109, 1 (Jan. 2008), pp. 69-85. DOI= http://dx.doi.org/10.1016/j.cviu.2007.03.001

[32] V. Zharkova, S. Ipson, A. Benkhalil, and S. Zharkov. “Feature recognition in solar images”, *Artifical Intelligence Review*, 23(3), 2005, pp. 209–266.

[33] ZTRACE Data set (MSU) [Online], Available: http://www.cs.montana.edu/angryk/SDO/data/TRACEbenchmark/ [Accessed: Jan 29, 2010]